Dynamic Stark effect on XUV-laser-generated photoelectron spectra: Numerical experiment on atomic hydrogen

Chuan Yu,* Ning Fu, Guizhong Zhang, and Jianquan Yao

College of Precision Instrument and Optoelectronics Engineering, Key Lab of Optoelectronic Information and Technology Science (Ministry of Education), Tianjin University, Tianjin 300072, P.R. China

(Received 19 March 2013; published 10 April 2013)

We present the results of our numerical simulation on the photoelectron spectra of hydrogen atoms ionized by the single-photon process of intense XUV laser pulses. The dynamic interference structure in the photoelectron spectra is investigated with respect to the dynamic Stark effect, XUV laser parameters, and properties of the ionization continuum states. The research outcome is that plane waves can be readily deployed to study photoelectron spectroscopy, which is crucial to the wave-function ansatz for generic systems of atoms and molecules. The dynamic Stark effect is prominently demonstrated above certain carrier frequencies of the XUV laser pulse, which mandates a photon energy threshold for the dynamic Stark effect to be discerned in the photoelectron spectra. A one-dimensional model for the hydrogen atom is feasible, which is of fundamental significance in modeling atoms and molecules with reduced dimensionality models. We also point out that detailed characterization of the interference fringes in the photoelectron spectra will facilitate more quantitative investigations of the Stark effect contained in the photoelectron spectra created by single XUV photons.

DOI: 10.1103/PhysRevA.87.043405 PACS number(s): 32.80.Rm, 82.50.Kx

I. INTRODUCTION

The past three decades have clarified the nature of intense laser interactions with atoms and molecules, and the light source has evolved from a nanosecond duration for excimer lasers and a femtosecond duration for Ti:sapphire lasers to a several-femtosecond pulse width for lasers in extreme ultraviolet (XUV) wavelengths [1–4]. The state-of-the-art XUV laser, the free electron laser, for instance, posseses a single-photon energy capable of overcoming the ionization threshold of any known atomic and molecular species. The theory and the relevant techniques inherent in single-photon events can readily be transplanted to treat the microprocesses induced by XUV light pulses in atoms and molecules [5–7]. Correspondingly, the numerical simulations start to burgeon for interactions of atoms and molecules lodged in a XUV laser field, simply because of the feasibility of experimental verification of the novel findings in theory.

The optical Stark effect [8,9], discovered a long time ago and serving as a proof for quantum mechanics, turns out to be a prominent process in almost all laser-atom and laser-molecule interactions. This phenomenon has been studied in both experimental and theoretical aspects for many decades [10], and it remains an interesting topic today. On one hand, the dynamic or ac Stark effect is an effective tool for quantum control of photochemical processes [11–13]. On the other hand, with the advent of ultrashort XUV laser pulses the dynamic Stark effect shows novel features. Chini *et al.* [14] investigated the subcycle ac Stark effect of helium atoms excited and probed with a combined pulse train of near-infrared (NIR) and XUV pulses; their finding was a subcycle energy level shift in helium. The pioneering work by Demekhin *et al.* [15] found for the first time that strong interference fringes emerge as new spectral feature in photoelectron spectra of hydrogen atoms excited with a XUV laser pulse of carrier frequency 53.6 eV which is far beyond the hydrogenic ionization potential of 13.6 eV. The dynamic interference effect was revealed to come from the dynamic Stark effect of a hydrogen atom mapped to the continuum via excitation of a single photon of XUV wavelength. The clear physical picture that the authors presented has shed much light on many future research contexts for the XUV excitation region.

Under appropriate conditions, the energy level shift induced by the dynamic Stark effect just follows in time the square of the envelope of the electric field of the laser pulse regardless of the carrier frequency [16]. Usually, the value of the second-order Stark shift is negative, meaning that the energy level is lowered in energy. For a hydrogen atom in its ground state, the dynamic Stark shift is, however, positive for the carrier frequency of 53.6 eV. This positive-value property of the dynamic Stark effect differs from the traditionally recognized negative-value property of the second-order Stark effect. Inspired by the above-threshold ionization process [17] revealed in studies on interaction of intense light with atoms and molecules, we tentatively believe that this phenomenon is of an intense field process, as illustrated by the modulation in the photoelectron spectra of hydrogen atoms exposed to an XUV laser field.

The novel property unique to XUV single-photon processes in atoms and molecules is that only the initial state and final state are involved, and the tedious intermediate states can be neglected due to the intrinsic selective nature of resonance excitation between the initial and the final states. The present work focuses on single-photon excitation of a hydrogen atom exposed to XUV light pulses of varying parameters, and on the variation of the modulation feature in the photoelectron spectra due to different formalisms of the final wave functions, which we select to be either the rigorous eigenfunction for the continuum states of the hydrogen atom or a simple plane wave. Meanwhile, the dipole transition moments associated with the XUV single-photon absorption process are examined

*chyu@tju.edu.cn

for their impact on the dynamic interference structure of the photoelectron spectra. Finally, we deduce our numerical simulation from the real three-dimensional (3D) hydrogen atom to a one-dimensional (1D) model for a hydrogen atom and compare the simulation outcomes with those inferred from the real 3D situation. In particular, we investigate the dynamic Stark effect and its influence on the photoelectron spectra by surveying the XUV laser frequency range over which the interference feature in the photoelectron spectra persists.

The paper is therefore organized as follows. Section II reports the theoretical and numerical aspects, Sec. III describes the computed results and discusses the outcomes, and Sec. IV wraps up paper with some remarks.

II. THEORY AND COMPUTATIONS

The microprocess of a hydrogen atom lodged in an intense XUV laser field is excitation from the ac Stark-shifted ground state to above-ionization-threshold continuum states. The ionization potential of a hydrogen atom is about 13.6 eV, which signifies, in a weak laser regime, that a single photon of energy 13.6 eV and higher can preferentially ionize the hydrogen atom and produce photoelectrons with a kinetic energy equal to the photon energy minus the ionization potential of 13.6 eV. In the strong XUV laser excitation case, however, the photoelectron spectra manifest themselves in interference fringes instead of a single peak. This novel phenomenon associated with XUV single-photon excitation was first demonstrated theoretically in Ref. [15] and was ascribed to the dynamic Stark effect of the ground state of the hydrogen atom, which was mapped to the ionization continuum states through the single-photon excitation process. In addition to a concise description of the numerical findings, the authors clarified the physical picture by clear derivations making use of the rotating-wave approximation (RWA) and the local approximation [18] for the analytical ansatz and proved that the coherent addition of electrons with equal energy but dislodged at different temporal moments resulted in blue-shift and modulation or interference fringes in the photoelectron spectra.

The formulas dictating the single-photon ionization process are pretty similar to the quantum wave-packet formalism [19] for molecules of nuclear motions on potential energy surfaces. Theoretically, the time-dependent wave function is expressed as a linear combination of the ground-state wave function and the continuum state ones, with nonessential states neglected:

$$|\psi(t)\rangle = a_I(t)|I\rangle + \sum_{j=1}^{N} \Delta\varepsilon a_{\varepsilon,j}(t)|F_{\varepsilon,j}\rangle \exp(-i\omega t). \tag{1}$$

The plugging of this wave function into the time-dependent Schrödinger equation and the projection onto each eigenstate give the coupled time-dependent equation set for the wave functions. By following Ref. [15] and using the RWA, we reformulate these coupled equations in discrete forms as follows [atomic units (a.u.) are used]:

$$i\dot{a}_I(t) = \sum_{j=1}^{N} \Delta\varepsilon \frac{1}{2} D^*_{\varepsilon,j} E_0 g(t) a_{\varepsilon,j}(t), \tag{2a}$$

$$i\dot{a}_{\varepsilon,j}(t) = \frac{1}{2} D_{\varepsilon,j} E_0 g(t) a_I(t) + (V_I + \varepsilon_j - \omega) a_{\varepsilon,j}(t). \tag{2b}$$

Here $|I\rangle$ is the ground state and $\left|F_{\varepsilon,j}\right\rangle$ is the final continuum state, with the energy of the photoelectron being ε_j. With the electric field of the XUV laser pulse polarized along the z axis, $D_{\varepsilon,j} = \left\langle F_{\varepsilon,j}\right| z \left|I\right\rangle$ is the energy-dependent dipole transition matrix element. V_I is the ionization potential of hydrogen ($V_I = 13.6$ eV). ω, E_0, and $g(t)$ are parameters of the XUV laser pulse, which is described as

$$E_L(t) = E_0 g(t) \cos(\omega t) = E_0 \exp(-t^2/\tau^2) \cos(\omega t). \tag{3}$$

By defining a state vector,

$$\mathbf{A}(t) = \{a_I, a_{\varepsilon,1}\sqrt{\Delta\varepsilon}, a_{\varepsilon,2}\sqrt{\Delta\varepsilon}, \cdots, a_{\varepsilon,N}\sqrt{\Delta\varepsilon}\}^T, \tag{4}$$

the Schrödinger equation (in the energy representation) simply reads

$$i\dot{\mathbf{A}}(t) = \mathbf{H}(t)\mathbf{A}(t). \tag{5}$$

Here $\mathbf{H}(t)$ is the Hamiltonian, which is a Hermitian matrix.

The initial and final wave functions are essential for calculating the dipole transition matrix element. We use the ground-state wave function of the real hydrogen atom in three dimensions for the initial state (atomic units are used for all following wave functions):

$$\phi_{100} = R_{10} Y_{00} = \pi^{-1/2} \exp(-r). \tag{6}$$

The final wave functions in the continuum are expressed for free electrons in the present calculation as (a) the rigorous eigenfunction for the continuum states of the hydrogen atom:

$$\phi_{klm} = R_{kl} Y_{lm}. \tag{7}$$

And R_{kl} takes a sophisticated expression [20],

$$\begin{aligned} R_{kl} = {} & \frac{1}{(2l+1)!} \frac{2\sqrt{k}}{1 - \exp(-2\pi/k)} \\ & \times \prod_{s=1}^{l} \sqrt{s^2 + k^{-2}} (2kr)^l \exp(-ikr) \\ & \times F(i/k + l + 1, 2l + 2, 2ikr), \end{aligned} \tag{8}$$

where $F(i/k + l + 1, 2l + 2, 2ikr)$ is the confluent hypergeometric function. Alternatively, the final wave functions can be expressed as (b) a simple plane wave propagating along the z axis:

$$\phi_k^{3D} = (2\pi)^{-3/2} \exp(ikz). \tag{9}$$

Both the functions given above are normalized to $\delta(k)$, and we normalize them to $\delta(\varepsilon)$ by multiplying them by $k^{-1/2}$ when calculating the dipole transition matrix element. In our calculation, only the $1s \rightarrow \varepsilon p$ transition is involved, i.e., we calculate $\langle \phi_{klm}|z|\phi_{100}\rangle$ and $\langle \phi_k^{3D}|z|\phi_{100}\rangle$. Note that k is the wave vector here.

We even extend our calculation to 1D hydrogen atoms and use the 1D plane wave for the final wave function:

$$\phi_k^{1D} = (2\pi)^{-1/2} \exp(ikz). \tag{10}$$

By using a soft-core [21] Coulomb potential,

$$V(z) = -1/\sqrt{2 + z^2}, \tag{11}$$

the initial wave function is numerically solved by the imaginary time relaxation method [22] and the corresponding ionization potential $V_I = 13.6$ eV is reproduced [23].

Although the plane wave is not strictly orthogonal to the ground-state wave function, it is still a proper choice for the final wave function in the continuum according to our simulation results. Besides, as an approximate expression for the wave function in the continuum, the plane wave can be adopted when the calculation of the dipole transition matrix element is extended to molecular systems whose wave functions can hardly be solved analytically.

In order to solve Eq. (5) and, further, to calculate the photoelectron spectrum, which is a plot of the norm squared on the ordinate versus the energy on the abscissa, we start from the initial state vector $\mathbf{A}(-\infty) = \{1,0,0,\ldots,0\}^T$ and evolve it in time. Equation (5) is solved through matrix diagonalization of the Hamiltonian. This algorithm is similar to the treatment of the potential matrix in wave-packet dynamics [19], which is fairly easy to implement.

Now we turn to the excitation light in XUV wavelength regime. Equation (3) gives the formula for the electric-field strength of the XUV pulse. For XUV laser pulses considered in our simulation, the intensity is varied from 1×10^{16} to 1×10^{17} W/cm^2, the pulse width τ in Eq. (3) is varied from 1 to 10 fs, and the carrier frequency ω is also made to vary from a value equal to the ionization threshold V_I to 80 eV, a value well above the threshold. Equation (3) gives the formula for the electric-field strength of the XUV pulse.

Pertaining to the computations, the energy grid for the continuum states is refined to confirm the reproduction of the computed results, thus corroborating the calculation precision.

III. RESULTS AND DISCUSSION

A. Influence of final continuum-state wave functions

Upon ionization from the ground state by an XUV laser pulse, the time-dependent wave function of the hydrogen atom can be expressed as the linear combination of the ground-state wave function and a number of continuum-state wave functions. Here we choose two kinds of wave functions for the final continuum-state electron, namely, the rigorous eigenfunction of Eq. (7) and the more conventional plane wave of Eq. (9).

In Fig. 1, we show the dipole transition moment functions that exist in Eqs. (2a) and (2b) and are used in the numerical simulation. For this part, we focus on the solid and dashed curves in the figure, while the dotted curve is referred to in Sec. III D.

Figure 2 demonstrates the photoelectron spectra under the excitation of an XUV laser field of pulse width $\tau = 3$ fs, with the intensity changed over a large range. One can unambiguously infer from these two sets of spectra that the spectra are characterized by the following common features: (i) spectral peaks are located at an energy higher than the the single-photon energy (53.6 eV) minus the hydrogen ionization potential ($V_I = 13.6$ eV), and the peaks shift to even higher energy positions with increasing laser intensity; (ii) a modulation structure exists due to the dynamic interference; (iii) more interference fringes appear with increasing XUV laser intensity; and (iv) different continuum-state wave functions demonstrate slightly different interference fringes, with the plane-wave wave function showing denser modulations. It is known that the eigenfunction for the continuum states is rigorously orthogonal to all the bound-state wave functions of the hydrogen atom; the resultant interference feature in

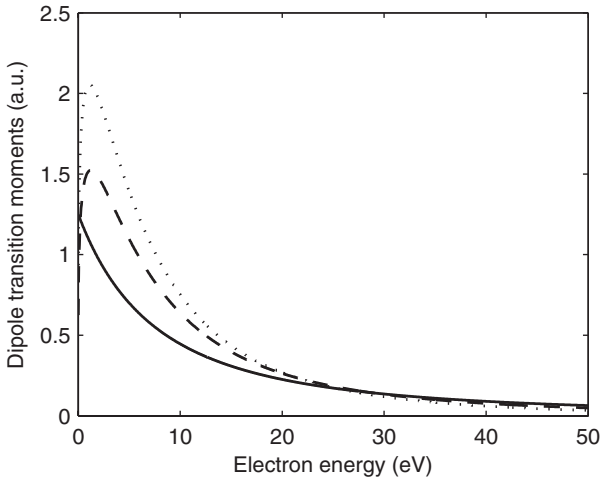

FIG. 1. A variety of dipole transition moments calculated and utilized in the present simulation of the dynamic Stark effect on the interference feature in the photoelectron spectra of a hydrogen atom exposed to XUV laser pulses. The solid curve represents the rigorous eigenfunction, and the dashed curve represents the plane wave as the final continuum-state wave function. The dotted curve represents the 1D hydrogen atom, which is discussed at the end of Sec. III. Note that the abscissa shows the value above the ionization threshold V_I of 13.6 eV.

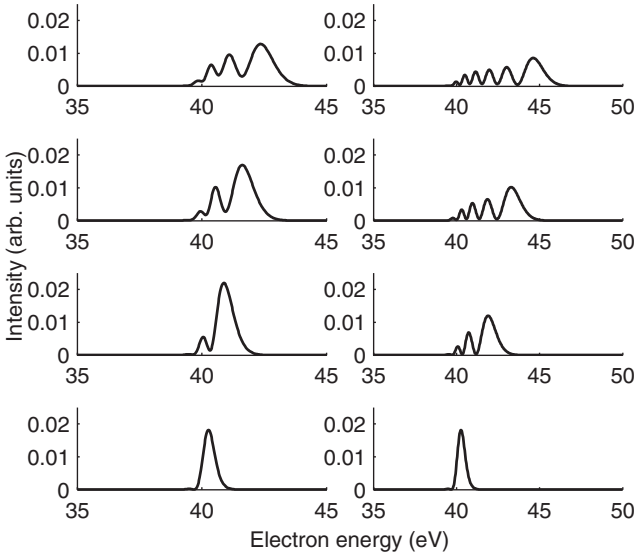

FIG. 2. Comparison of the photoelectron spectra of a hydrogen atom excited from the ground state to final continuum states, which are expressed by the rigorous eigenfunction (left) or plane-wave function (right). The XUV laser pulse is used at a carrier frequency of 53.6 eV. The XUV laser intensity is 1×10^{16}, 3×10^{16}, 5×10^{16}, and 7×10^{16} W/cm^2, respectively, from the bottom curve to the top. The pulse width $\tau = 3$ fs.

the photoelectron spectra should, therefore, be closer to the to-be-measured spectra under XUV excitation. As a fairly good alternative, the plane waves can be readily deployed to represent wave functions for free electrons in the ionization continuum. The applicability of the plane-wave wave function is also demonstrated in addressing the reduced-dimensionality case for the hydrogen atom. It has been determined [15] that the interference feature in the photoelectron spectra arises from the dynamic Stark effect of the ground state of the hydrogen atom. Beyond this finding, one clearly discerns that the modulated spectra shift as a whole to the blue region which the dynamic Stark effect predominates, because the dynamic Stark shift is about 2.6 eV for a laser intensity of 5×10^{16} W/cm^2. We edify ourselves that this phenomenon is of an intense light nature like the well-recognized above-threshold ionization process. What contrasts most with the perturbative theory of the second-order Stark effect is the energy level up-shift to a positive value for intense XUV laser excitation. Although more investigation into the detailed interference structure in the photoelectron spectra and its relation to the XUV laser properties is certainly needed, we anticipate that the plane-wave approximation can be effective in coping with the free electrons in ionization continuum states.

We also seek the temporal development of the photoelectron spectra over the entire pulse period of the XUV interaction with the hydrogen atom. Figure 3 gives these time variations of the peak appearance and peak shifting. This figure hints that time-resolved spectroscopy of the photoelectron spectra can provide dynamic evolution information on strongly modulated spectra. And one can always obtain the spectrally resolved feature in the photoelectron spectra with more conventional spectroscopy, which are the temporally sliced spectra at infinite time. We find similar peak emerging and peak shifting trends for both of the final wave functions discussed above, and the final wave function used for computation in Fig. 3 is the plane wave. It is obvious from Fig. 3 that the interference feature gradually appears and shifts to higher energy locations as the XUV laser pulse ascends, peaks, and descends in time, eventually forming the observed spectra with strong modulation shown in Fig. 2.

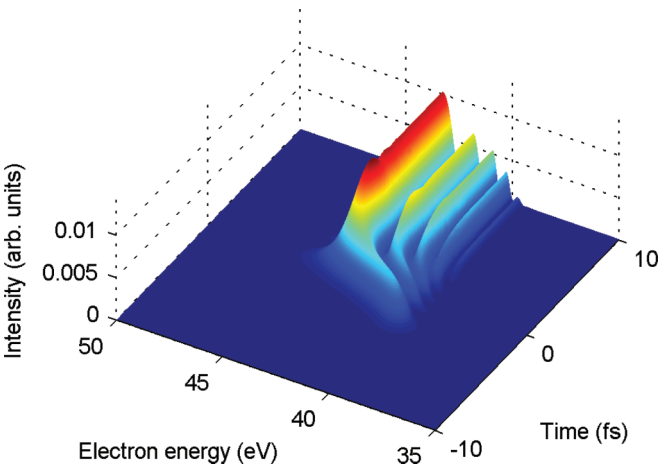

FIG. 3. (Color online) Dynamic development of the inference feature in the photoelectron spectra. Simulation parameters are laser intensity $= 5 \times 10^{16}$ W/cm^2, XUV laser pulse carrier frequency $\omega =$ 53.6 eV, and laser pulse width $\tau = 3$ fs. One can read that at early stages the peak emerges at around the energy position of the carrier frequency minus the ionization potential, and more peaks burgeon and simultaneously blue-shift as the laser pulse dumps more energy into the hydrogen atom.

B. Influence of the XUV laser pulse

The above discussion demonstrates a clue to the laser intensity dependence of the modulation structure in the photoelectron spectra. In order to gain a systematic insight into the influence of the XUV laser pulse on the photoelectron spectra, we perform extensive numerical simulation of the modulation-characterized photoelectron spectra by focusing on the laser parameters and their impact on the interference feature in the spectra.

Figure 4 shows typical photoelectron spectra intended to demonstrate the dependence of the interference feature on the pulse duration and carrier frequency of the XUV pulse used. The modulated spectral curves, as given in the left panel in Fig. 4, unambiguously reflect that the interference fringes depend on the pulse duration in a monotonic way: the longer the pulse, the more fringes the spectra bear. This kind of numerically observed behavior can be understood in terms of the RWA and the local approximation, as given in Ref. [15]. An analytical formula derived in Ref. [15] was used to estimate the accumulated phase by the two interfering electronic wave packets over the entire XUV pulse duration. To be simple, this phase accumulation is proportional to the laser pulse width and to the dynamic Stark shift value, and every phase increment of 2π will map a crest and a trough in the photoelectron spectra. Our computed results, given in the left panel in Fig. 4, corroborate the analytical theory [15] that

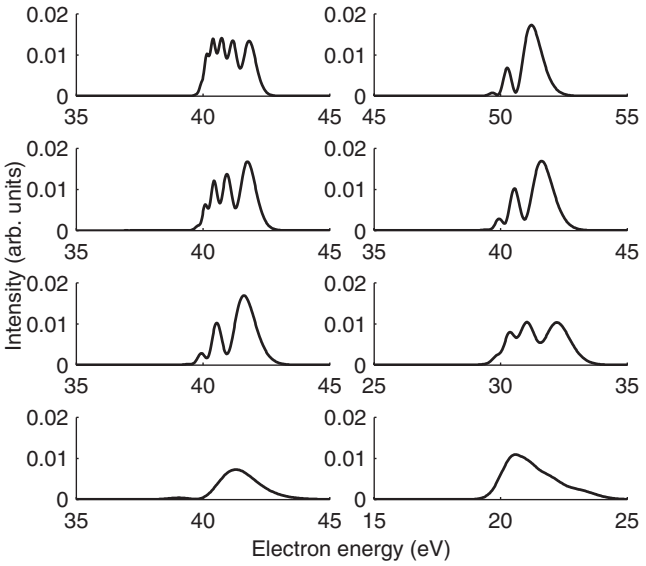

FIG. 4. Dependence of the spectral interference fringes in the photoelectron spectra on the laser carrier frequency and duration for an intensity of 5×10^{16} W/cm^2. Left: Varying pulse widths of 1, 3, 5 and 7 fs from the bottom to the top curve. Right: Varying carrier frequencies of $V_I + 20$ eV, $V_I + 30$ eV, $V_I + 40$ eV, and $V_I + 50$ eV from the the bottom to the top curve. Note that the ionization potential $V_I = 13.6$ eV.

the number of interference fringes in the photoelectron spectra scales with the pulse width.

The pioneering work [15] on the interference structure of the photoelectron spectra has revealed the spectral nature of the dynamic Stark effect. It is known that the dynamic Stark effect is only dependent on the square of the pulse envelope, independent of the carrier frequency, of an intense laser pulse under certain conditions [16]. The spectral curves shown in the right panel in Fig. 4 are plotted for varying carrier frequencies above the ionization potential of 13.6 eV. It is very clear that all the simulated spectra except for the lowest carrier frequency situation have similar spectral features of interference fringes, and differences do exist. With increasing carrier frequency, the spectral spread of the photoelectron spectra becomes narrower and narrower while the dynamic Stark effect fades out for the lowest carrier frequency used.

According to Ref. [15], the ac Stark shift can be expressed in the form of a principal value integral. Here we rewrite it in the discrete form under the RWA and calculate its value numerically:

$$\Lambda = \left[-\sum_{j=1}^{N} \Delta\varepsilon |D_{\varepsilon,j}|^2 \frac{E_0^2}{4} \left(\frac{1}{V_I + \varepsilon_j - \omega} \right) \right]. \quad (12)$$

This integration will yield positive values for sufficiently large ω values. When the value of ω is decreased, however, the integration will become 0 and eventually negative. Our calculation of the dynamic Stark shift Λ for the carrier frequency of 53.6 eV and the intensity of 5×10^{16} W/cm^2 yields a value of 2.6 eV. The interference fringes will accordingly fade out as the dynamic Stark shift goes to 0, which explains the disappearance of the modulation in the photoelectron spectrum shown by the bottom curve in the right panel in Fig. 4.

C. Impact of the dipole transition function

As shown in Eq. (12), the dipole transition moment, which serves as the coupling between the ground state and the continuum states, is also crucial to the dynamic Stark effect. Figure 5 demonstrates the variations of the photoelectron spectra calculated for different forms of the dipole transition moment. The left panel in Fig. 5 shows the dipole transition moments and the right panel shows the resultant photoelectron spectra. As for the dipole transition moments, one curve is simply a flat function, while most others are similar to each other but shifted to different energy positions along the energy axis.

What can be clearly discerned from Fig. 5 is the overall spectral shift to higher energy positions, the overall spectral broadening, and the intensification of the lower energy interference fringes in the spectra as the dipole transition moment functions peak at higher energy positions. It is reasonable to imagine that the overall photoelectron spectra shift, as a whole, to higher energy positions for the dipole transition moment functions peaking at higher energy locations in a certain range.

Particularly, the photoelectron spectra corresponding to the flat dipole transition moment function only manifest a single broad peak without interference fringes. This can be deciphered by studying Eq. (12); i.e., the flat dipole transition moment function weakens the dynamic stark effect, thus mapping no interference fringes in the photoelectron spectra.

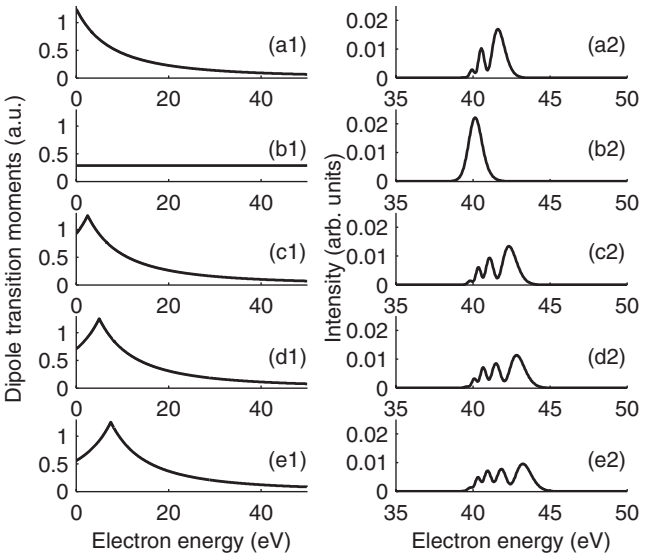

FIG. 5. Performance of the photoelectron spectra simulated for quite varying dipole transition functions between the initial ground-state and the final continuum states. Left: Dipole transition moments. Right: Resultant photoelectron spectra. The curve in (a1) is the same as the solid curve in Fig. 1. By taking its average value we obtain the curve in (b1). The curves in (c1), (d1), and (e1) are formulated by right-shifting the curve in (a1) by 2.5, 5.0, and 7.5 eV, respectively. The most prominent property is the blue shift and spectral broadening of the interference structures for dipole transition moment functions peaking at higher and higher energy locations.

As for the detailed variations of the relative intensities of the individual interference fringes, we have not found a consistent explanation yet.

D. Reduction to one dimension

For many decades, 1D [24–27] or 2D [28,29] models have often been used in the numerical simulation of intense laser interaction with atoms and molecules because reduced-dimensionality model studies can maintain the essential physics while weakening the computational burdens considering the computer capabilities nowadays.

In Fig. 6 we plot two panels of spectra for comparison. The left panel is for a real 3D hydrogen atom with exact wave functions for both the bound ground state and the free continuum states (rigorous eigenfunction), and the right panel is for the 1D hydrogen atom model for which the ground-state wave function is calculated for this model and the free continuum-state wave functions take the plane wave.

The spectral curves in Fig. 6 are read in two aspects: the 1D model for a hydrogen atom exhibits modulation structures, spectral blue-shifting and spectral broadening with increasing laser intensities, which are qualitatively similar to those of the real 3D hydrogen atom; the 1D model demonstrates more interference fringes and broader spectra than its counterpart in the 3D case. We have conducted the simulation of the temporal development of the photoelectron spectra for a 1D hydrogen

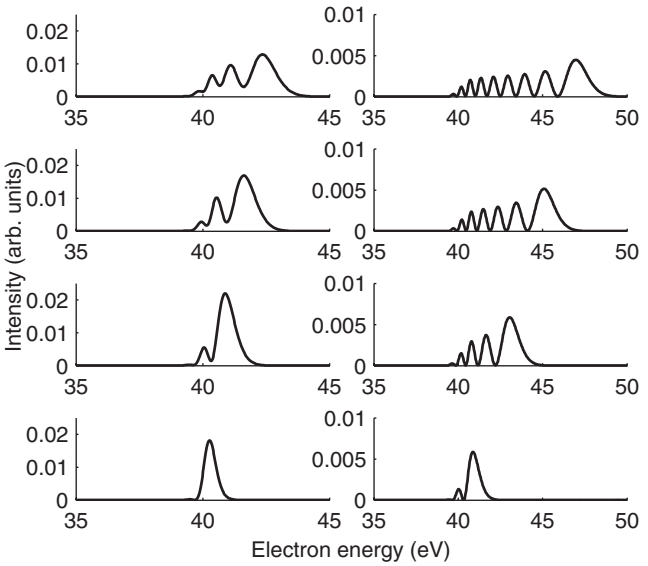

FIG. 6. Comparative plots for the spectral feature of the photoelectron spectra of a real 3D hydrogen atom (left) and a 1D-model hydrogen (right), both excited by an XUV laser pulse of a carrier frequency of 53.6 eV. The XUV laser intensity is 1×10^{16}, 3×10^{16}, 5×10^{16}, and 7×10^{16} W/cm^2, respectively, from the bottom to the top curve. Pulse width $\tau = 3$ fs.

over the entire XUV laser pulse duration and found modulation fairly similar to that in Fig. 3.

Usually, the excitation laser is linearly polarized along a certain direction; this property facilitates the feasibility of the dimension reduction to 1D models. A variety of 1D models [24–27] have been proposed and tested for investigation of atom and molecule interactions with intense laser light. The abundant interference fringes shown in the photoelectron spectra simulated for the 1D hydrogen model in Fig. 6 are mainly ascribed to the adoption of the plane waves as the final-state wave functions; this is also confirmed for the real 3D hydrogen atom, showing denser modulation in the photoelectron spectra for the plane-wave wave functions than for the rigorous eigenfunction (Fig. 2).

Reference [15] discussed the accumulated phase value from the viewpoint of the RWA and the local approximation; we also used their formula for discussing the number of interference fringes, as the accumulated phase is proportional to the dynamic Stark effect value and the pulse width. Figure 4 also shows that the carrier frequency of the XUV laser might be a dominant factor in forming the concrete pattern of interference in the photoelectron spectra. The numerically observed spectral feature in the photoelectron awaits experimental verification before further theoretical work is needed.

IV. CONCLUDING REMARKS

Our extensive simulations of the interference feature that emerges in the photoelectron spectra of a hydrogen atom ionized to the continuum states by the single-photon process of intense XUV laser pulses reveal that the dynamic Stark effect, XUV laser parameters, and atomic properties of the target atom all contribute to the modulation structure in the photoelectron spectra. Being widely used in numerical experiments on the interaction of intense laser pulses with atoms and molecules, reduced-dimensionality models, in one or two dimensions, are feasible workbenches for computation of the dynamic interference behavior of hydrogen atoms, which maintains the essential physics while mitigating the computational workload. The simple formalism of a plane-wave wave function can be an effective alternative for elucidating the free electrons in the ionization continuum. We are also convinced that the interference feature in the photoelectron spectra depends on the laser carrier frequency and atomic properties, and the spectral modulation is prominent for a high enough single-photon energy. Our anticipation is that more detailed investigation of the interference fringes in the photoelectron spectra will help shed light on the single-photon process entangled by the dynamic Stark effect.

ACKNOWLEDGMENT

The authors acknowledge the support by the NSFC of China through Contract No. 10674100.

[1] L. Fang, T. Osipov, B. Murphy, F. Tarantelli, E. Kukk, J. P. Cryan, M. Glownia, P. H. Bucksbaum, R. N. Coffee, M. Chen, C. Buth, and N. Berrah, Phys. Rev. Lett. **109**, 263001 (2012).
[2] M. Nagasono, E. Suljoti, A. Pietzsch, F. Hennies, M. Wellhöfer, J.-T. Hoeft, M. Martins, W. Wurth, R. Treusch, J. Feldhaus, J. R. Schneider, and A. Föhlisch, Phys. Rev. A **75**, 051406 (2007).
[3] A. Palacios, H. Bachau, and F. Martín, Phys. Rev. A **75**, 013408 (2007).
[4] A. A. Sorokin, M. Wellhöfer, S. V. Bobashev, K. Tiedtke, and M. Richter, Phys. Rev. A **75**, 051402 (2007).
[5] W. Li, R. R. Lucchese, A. Doyuran, Z. Wu, H. Loos, G. E. Hall, and A. G. Suits, Phys. Rev. Lett. **92**, 083002 (2004).
[6] P. V. Demekhin and L. S. Cederbaum, Phys. Rev. A **83**, 023422 (2011).
[7] P. V. Demekhin, Y.-C. Chiang, and L. S. Cederbaum, Phys. Rev. A **84**, 033417 (2011).
[8] S. H. Autler and C. H. Townes, Phys. Rev. **100**, 703 (1955).
[9] A. Bonch-Bruevich, N. Kostin, V. Khodovoi, and V. Khromov, Sov. Phys. JETP **29**, 82 (1969).
[10] N. B. Delone and V. P. Krainov, Phys. Usp. **42**, 669 (1999).
[11] B. J. Sussman, D. Townsend, M. Y. Ivanov, and A. Stolow, Science **314**, 278 (2006).
[12] B. J. Sussman, J. G. Underwood, R. Lausten, M. Y. Ivanov, and A. Stolow, Phys. Rev. A **73**, 053403 (2006).
[13] Y.-C. Han, K.-J. Yuan, W.-H. Hu, and S.-L. Cong, J. Chem. Phys. **130**, 044308 (2009).
[14] M. Chini, B. Zhao, H. Wang, Y. Cheng, S. X. Hu, and Z. Chang, Phys. Rev. Lett. **109**, 073601 (2012).

[15] P. V. Demekhin and L. S. Cederbaum, Phys. Rev. Lett. **108**, 253001 (2012).
[16] B. J. Sussman, Am. J. Phys. **79**, 477 (2011).
[17] J. Eberly, J. Javanainen, and K. Rzaewski, Phys. Rep. **204**, 331 (1991).
[18] L. S. Cederbaum and W. Domcke, J. Phys. B **14**, 4665 (1981).
[19] B. M. Garraway and K. A. Suominen, Rep. Prog. Phys. **58**, 365 (1995).
[20] L. D. Landau and E. M. Lifshitz, *Quantum Mechanics: Non-relativistic Theory*, 3rd ed. (Pergamon Press, New York, 1977).
[21] J. Javanainen, J. H. Eberly, and Q. Su, Phys. Rev. A **38**, 3430 (1988).
[22] R. Kosloff and H. Tal-Ezer, Chem. Phys. Lett. **127**, 223 (1986).
[23] J. B. Watson, A. Sanpera, D. G. Lappas, P. L. Knight, and K. Burnett, Phys. Rev. Lett. **78**, 1884 (1997).
[24] H. Yu, T. Zuo, and A. D. Bandrauk, Phys. Rev. A **54**, 3290 (1996).
[25] N. A. Nguyen and A. D. Bandrauk, Phys. Rev. A **73**, 032708 (2006).
[26] M. Thiele, E. K. U. Gross, and S. Kümmel, Phys. Rev. Lett. **100**, 153004 (2008).
[27] A. D. Bandrauk, S. Chelkowski, P. B. Corkum, J. Manz, and G. L. Yudin, J. Phys. B **42**, 134001 (2009).
[28] M. Lein, N. Hay, R. Velotta, J. P. Marangos, and P. L. Knight, Phys. Rev. Lett. **88**, 183903 (2002).
[29] M. Odenweller, N. Takemoto, A. Vredenborg, K. Cole, K. Pahl, J. Titze, L. P. H. Schmidt, T. Jahnke, R. Dörner, and A. Becker, Phys. Rev. Lett. **107**, 143004 (2011).